ACS SENSORS

Editors' Choice
Open Access
This article is licensed under CC-BY-NC-ND 4.0
pubs.acs.org/acssensors

Article

A Biohydrogel-Enabled Microneedle Sensor for In Situ Monitoring of Reactive Oxygen Species in Plants

Nawab Singh, Qinming Zhang, Weihui Xu, Steven A. Whitham, and Liang Dong*

Cite This: https://doi.org/10.1021/acssensors.4c02645

Read Online

ACCESS | Metrics & More | Article Recommendations | Supporting Information

ABSTRACT: This study introduces a plant sensor utilizing an array of microneedles to monitor hydrogen peroxide (H_2O_2) in tobacco and soybean plants under biotic stress response. The microneedle array features a biohydrogel layer composed of the natural biopolymer chitosan (Cs) and reduced graphene oxide (rGO), functionalized with horseradish peroxidase (HRP) (HRP/Cs-rGO). This HRP/Cs-rGO biohydrogel combines biocompatibility, hydrophilicity, porosity, and electron transfer ability, making it a suitable bioelectrode material for an electrochemical sensor. The sensor detects H_2O_2 through the catalytic reaction of the enzyme, either by direct attachment to the plant leaf with the inserted microneedle or by exposure to the solution extracted from plant parts such as leaves. Utilizing chronoamperometry, the sensor demonstrates high sensitivity of 14.7 μA/μM across a concentration range of 0.1−4500 μM with a low detection limit of 0.06 μM. The sensor enables rapid detection of H_2O_2 levels by exposing the sensor to extracted leaf solutions. For in situ measurements within the leaf, results are obtained in approximately 1 min, eliminating the need for sample preparation. H_2O_2 levels in leaves following bacterial pathogen inoculation are evaluated alongside results from qualitative histological staining and quantitative fluorescence-based Amplex Red Assay, validating the ability of the sensor to detect changes in H_2O_2 concentrations during plant defense responses. This sensor technology has the potential to function as a portable device for on-site measurement of reactive oxygen species in plants, providing a rapid and cost-effective solution for H_2O_2 quantification.

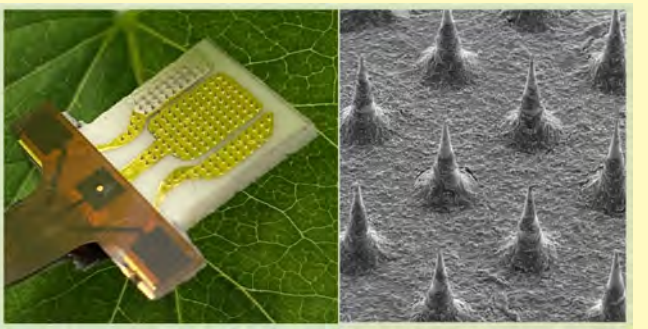

KEYWORDS: *plant sensor, plant science, biohydrogel, reactive oxygen species, biosensor*

Downloaded via IOWA STATE UNIV on March 26, 2025 at 16:50:58 (UTC).
See https://pubs.acs.org/sharingguidelines for options on how to legitimately share published articles.

Climate change exacerbates both biotic and abiotic stresses on crops, negatively impacting their yield.[1−3] Real-time monitoring of physiological conditions is essential for a better understanding of plant responses to various stresses.[3−7] Reactive oxygen species play a key role in cell-to-cell communication and activating plant defense mechanisms.[8,9] Hydrogen peroxide (H_2O_2) is particularly important for rapid signal transduction and serves as an indicator of acute stress.[10,11] Stressors like drought, temperature extremes, salinity, mechanical injuries, and pathogen infections can significantly impact H_2O_2 production, triggering regulatory responses.[12] Monitoring H_2O_2 levels in various plant parts, such as roots, petioles, and leaves, can provide valuable insights into stress responses and help decision-making for agricultural management.

Conventional methods for measuring H_2O_2 in plant samples include fluorescence method, histochemical staining method, colorimetry, and chemiluminescence.[12−17] These techniques, however, require relatively time-consuming sample preparation procedures and expensive instruments, can alter H_2O_2 levels, and face interference from chlorophyll autofluorescence, making them unsuitable for on-site measurement.[18−20] To address these issues, several inexpensive H_2O_2 biosensors have been developed.[3,21,22] For instance, a near-infrared fluorescent biosensor using single-walled carbon nanotubes (SWCNTs) functionalized with H_2O_2-selective DNA has enabled the monitoring of wound-induced H_2O_2 signals in plants.[12] An H_2O_2 sensor based on SWCNTs functionalized with a DNA aptamer that binds to hemin was also developed.[21] Additionally, H_2O_2 detection has also been realized using a metal−organic framework-based biosensor featuring color-to-thermal signal conversion,[3] as well as using single-chirality near-infrared fluorescent carbon nanotubes.[22] Despite these advancements, challenges such as autofluorescence interference and cross-reactivity with other compounds in plant tissue continue to hinder the practical application of these sensors.

Due to their high sensitivity and compactness, electrochemical sensors offer a promising solution for H_2O_2

Received: September 25, 2024
Revised: February 4, 2025
Accepted: March 3, 2025

© XXXX The Authors. Published by American Chemical Society

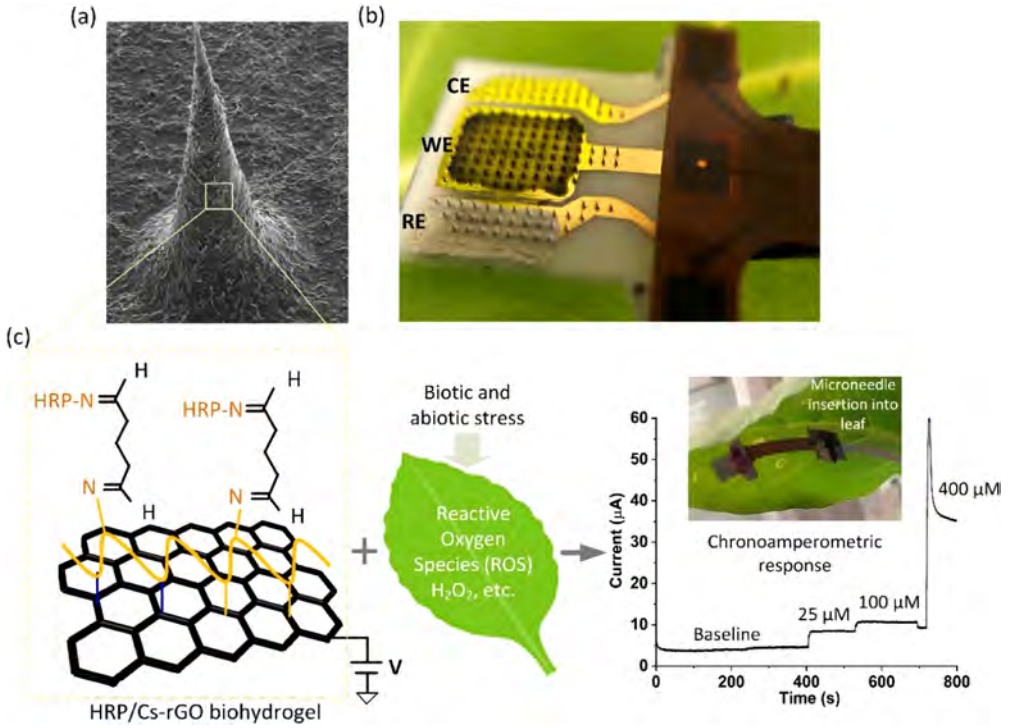

Figure 1. A biohydrogel-based microneedle sensor for in situ monitoring of H_2O_2 in plants. (a) Scanning electron microscope (SEM) image of an Au-coated microneedle functionalized with HRP/Cs-rGO biohydrogel. (b) Photograph of the fabricated microneedle sensor designed for in situ detection of reactive oxygen species (H_2O_2) in plant leaves. The sensor consists of working electrode (WE), counter electrode (CE), and reference electrode (RE), all formed using microneedle needles. The WE is functionalized with HRP/Cs-rGO biohydrogel, the RE is modified with Ag/AgCl, and the CE features a bare Au layer. (c) Schematic illustration depicting the chemical structure of HRP/Cs-rGO biohydrogel and its interaction with H_2O_2 within the leaf, resulting in an electrochemical current measured by chronoamperometry. The inset on the right shows the sensor attached to a leaf for H_2O_2 detection.

measurement in plants.[23,24] Recently, a Pt wire-based microelectrode was inserted into a quartz glass capillary coated with silver epoxy, and the tip of the assembled device was polished to create a two-electrode electrochemical sensor for in situ detection of H_2O_2 in *Agave tequilana* leaves. However, the device fabrication and integration process, along with the need for a three-dimensional micropositioner to facilitate measurement, introduced challenges in scalability and practical operation.[25] In addition, a paper-based sensor with a modified indium tin oxide working electrode has been reported for the detection of H_2O_2 in collected tomato leaf samples. However, its integration is not optimal, requiring the assembly of external reference and counter electrodes with the working electrode, and applying a phosphate buffer solution to the electrode surface covered with a piece of filter paper.[26] Another innovative sensor for plant H_2O_2 measurement employed a hollow microneedle array patch to extract plant fluid, which was then used to wet a filter paper interfaced with a separate screen-printed electrochemical H_2O_2 sensor. While this design enabled point-of-need testing for in situ plant monitoring, it required integrating multiple components and relying on thumb pressure applied to the leaf to extract a sufficient fluid volume for sensing.[27] Additionally, a sensor for detecting H_2O_2 in tomato leaves was developed using a stainless-steel wire modified with gold nanoparticles, along with a platinum wire and a silver/silver chloride (Ag/AgCl) wire. While this design allowed for precise measurements within the leaf vein, it required assembling three separate thin wires and carefully inserting them into the vein, a challenging task due to the small sizes of both the wires and the vein. Therefore, despite these advances, challenges remain in optimizing the design of sensors for in situ H_2O_2 monitoring for plants.[28]

Recently, conducting hydrogels have been integrated into various electrochemical sensing electrodes to enhance their sensitivity. This integration is demonstrated in the development of metabolite and glucose biosensors using platinum nanoparticles and polyaniline hydrogel,[29,30] living cell detectors featuring a conductive hydrogel made of polypyrrole and sulfonated multiwalled carbon nanotubes,[31] and ammonia and urea biosensors based on a hydrogel comprising acrylic acid and 2-(dimethylamino)ethyl methacrylate.[32,33] However, most hydrogel-based electrochemical sensors face challenges such as low instability attributed to their use of synthetic polymer-based hydrogels. The lack of biocompatibility in these synthetic hydrogels can also lead to cytotoxicity or immune responses due to their interactions with biological components. Additionally, the complexity of synthesizing synthetic conducting hydrogels poses obstacles to large-scale production.[34,35]

This study presents a biohydrogel-based microneedle sensor for direct in situ detection of H_2O_2 concentrations in plants (Figure 1). This sensor is designed to be attached to a plant leaf, with its microneedles penetrating the plant tissue, enabling electrochemical H_2O_2 detection without requiring leaf sap extraction or external detection methods. The microneedle surface is coated with a thin gold (Au) layer and further modified with a biohydrogel composed of naturally biocompatible and hydrophilic chitosan (Cs),[36] rGO, and horseradish peroxidase (HRP) enzyme (Figure 1a,b). This HRP/Cs-rGO (horseradish peroxidase/chitosan-reduced graphene oxide)

https://doi.org/10.1021/acssensors.4c02645
ACS Sens. XXXX, XXX, XXX−XXX

biohydrogel catalyzes the reaction of H_2O_2 at the HRP/Cs-rGO/Au-based working electrode (WE), generating electrochemical current changes for quantification (Figure 1c). The incorporation of Cs prevents rGO agglomeration by leveraging electrostatic interactions between cationic Cs and anionic rGO, facilitating the formation of a uniform Cs-rGO coating on the Au surface. The Cs-rGO hydrogel enables effective immobilization of HRP enzyme through imine binding. Additionally, rGO enhances the electrochemical sensing properties of the Cs-rGO/Au electrode compared to the Cs/Au electrode alone. This study demonstrates that HRP/Cs-rGO-coated microneedle sensor can effectively monitor H_2O_2 levels in tobacco and soybean plants during defense responses to bacterial infections.

Microneedle sensors have been widely developed for biomedical applications, such as detecting H_2O_2 released from cells and monitoring glucose levels in human skin interstitial fluid (SIF).[37] Additionally, swellable hydrogel-based microneedles have been reported for colorimetric detection of glutathione biomarkers,[38] while double-layer hydrogel microneedle patches have been employed for in situ glucose detection in SIF.[39] In plant science, microneedle technology has also been explored, but with limitations. One approach utilized a microneedle patch for rapid leaf sap extraction, requiring an external portable colorimeter for H_2O_2 detection.[40] Another a microneedle-based sensor was developed to detect salicylic acid using molecularly imprinted polymer technology.[41] In contrast, the plant sensor presented in this study integrates a biocompatible HRP/Cs-rGO biohydrogel onto the microneedle surface, enabling in situ electrochemical H_2O_2 detection without sample preparation or external measurement instrumentation, providing a more efficient solution for H_2O_2 detection in the plant.

EXPERIMENTAL SECTION

Chemicals. All chemicals used were of analytical grade, and deionized (DI) water (18.6 MΩ) was used in all experiments. Hydrofluoric acid (HF) and 30% H_2O_2 were procured from Fischer Scientific (Waltham, MA, USA). Au etchant (GE-8148) was obtained from Transene Electronic Chemicals (Danvers, MA, USA). Graphite powder, low molecular weight chitosan (Product No.: 448869), and HRP were purchased from Sigma-Aldrich (St. Louis, MO, USA). Phosphate-buffered saline (PBS; 10 mM, pH 7.4) was prepared using sodium dihydrogen phosphate, sodium monohydrate phosphate, and sodium chloride, all sourced from Sigma-Aldrich (St. Louis, MO, USA).

Synthesis of HRP/Cs-rGO Biohydrogel. The major methods with schematic for preparing the HRP/Cs-rGO biohydrogel are illustrated in Figure S1. For the synthesis of HRP/Cs-rGO biohydrogel, rGO was prepared using a modified Hummer's method.[43] A 0.5% aqueous acetic acid solution of Cs and an aqueous dispersion solution of rGO (0.5 mg/mL) were prepared separately; each dispersion solution was stirred at 500 rpm for 12 h at 25 °C. Next, the rGO dispersion solution was ultrasonicated for 2 h. Then, 500 μL of the rGO solution was mixed with 1 mL of the Cs solution and stirred at 500 rpm for 12 h. The mixture of rGO and Cs transformed into Cs-rGO hydrogel through electrostatic attraction between the cationic amino groups of Cs and the anionic surface of rGO (Figure S1a). Notably, rGO alone tends to exhibit poor dispersion in aqueous solutions. Incorporating Cs, a natural biopolymer,[43] mitigated rGO agglomeration and promoted the formation of a uniform coating on Au electrode surfaces. The resulting Cs-rGO hydrogel served as a uniform matrix for enzyme immobilization (Figure S1b).

To load the HRP enzyme, 50 μL of 1% glutaraldehyde (GA) solution was added to 500 μL of Cs-rGO solution and stirred at 500 rpm for 30 min at 25 °C. Next, 50 μL of HRP enzyme (4 mg/mL) was added to the GA-Cs-rGO hydrogel and stirred for another 30 min. The resulting HRP/Cs-rGO biohydrogel was kept on a shaker plate at 300 rpm for 2 h at 4 °C. The efficient loading of HRP enzyme molecules onto the Cs-rGO hydrogel surface was facilitated by the presence of amine, carboxylic, and hydroxy groups in the Cs-rGO hydrogel structure (Figure S1b). The prepared HRP/Cs-rGO biohydrogel was drop-cast onto the Au electrode surface and stored at 4 °C. An optimization study was performed to assess various combinations of Cs and rGO with HRP enzyme on the chronoamperometric (CA) responses of HRP/Cs-rGO/Au-based electrodes to H_2O_2. Details of the optimization experiment are provided in Supporting Information and Figure S4.

Sensor Fabrication. The fabrication process for the microneedle sensor started with creating an array of polyurethane-based microneedles using a two-step molding method. First, a computer-aided design containing the microneedles, featuring a needle height of 700 μm, a base diameter of 300 μm, and an apex diameter of 2 μm, was printed with IP-Q epoxy on the surface of a silicon substrate using a two-photon polymerization technique (Nanoscribe Photonic Professional GT2 3D printer; Nanoscribe GmbH & Co., Karlsruhe, Germany). The printed epoxy microneedles served as a positive mold for making a negative mold of polydimethylsiloxane (PDMS). In this process, the silicone elastomer base and its curing agent (SYLGARD 184 Silicone Elastomer Kit; Dow Corning Co., Midland, MI, USA), in a weight ratio of 10:1, were mixed and stirred. After degassing for 30 min, the PDMS solution was poured over the positive mold and cured at 80 °C for 2 h. The cured PDMS was then peeled off from the positive mold, thus forming the negative mold.[44] Subsequently, a two-part polyurethane mixture (components A and B in a weight ratio of 1:1; BJB Enterprises, Tustin, CA, USA) was stirred. The mixed solution was then applied to the PDMS negative mold, degassed for 10 min, and cured for 12 h at 23 °C. The cured structure was demolded from the PDMS mold, thus forming the polyurethane-based microneedle array. Next, a 200 nm-thick Au layer was deposited onto the microneedle array through a shadow mask using e-beam evaporation (Denton Explorer, Denton Vacuum, Moorestown, NJ). The working electrode (WE; 4 mm × 5 mm) was surrounded by a counter electrode (CE) and a reference electrode (RE). A 200 μm-thick layer of Ag/AgCl paste (E2414 AG/AGCL Ink; Ercon; Wareham, MA, USA) was screen-printed onto the RE using a screen printer, followed by thermal treatment on a hot plate (PC-420D; Corning Inc., Corning, NY) at 95 °C for 90 min. Finally, a flexible polyimide printed circuit board (PCB; OSH Park, Lake Oswego, OR) was attached by soldering the connectors to the PCB pads and then applying conductive epoxy (Chemtronics CW2400; Circuit Works, Waukegan, IL) on the PCB pads. Further, the WE surface was modified using the prepared HRP/Cs-rGO biohydrogel solution. In this step, 20 μL of the solution was drop-casted onto the WE surface and left to sit for 12 h at 4 °C, forming a layer of HRP/Cs-rGO biohydrogel on the WE surface. The device was then washed with a PBS solution (10 mM, pH 7.4) and stored at 4 °C for further use.

Plant Growth, Bacterial Infiltration, and Leaf Extract Preparation. Soybean (*Glycine max* cv. Williams 82) and tobacco (*Nicotiana tabacum* cv. Xanthi nc) plants were grown at an average temperature of 25 °C with 16 h of light. *Pseudomonas syringae* pathovar *tomato* DC3000 (*Pto* DC3000) was cultured overnight at 30 °C and harvested by centrifugation at 5000 g for 10 min at 20 °C. The supernatant was discarded, and the pellet was suspended with 10 mM $MgCl_2$ at an OD_{600} = 0.3. The bacterial suspension was inoculated by dipping or infiltration for soybean and tobacco, respectively. 3,3′-Diaminobenzidine (DAB; TCI, Portland, OR) staining for H_2O_2 detection was performed 24 h after inoculation as previously described.[45,46]

To induce H_2O_2 production, tobacco and soybean plants were Inoculated with fresh *Pto* DC3000 cultures prepared on King's B (KB) media supplemented with 50 μg/mL of rifampicin. Leaves were crushed to obtain liquid samples from 6 to 8-week-old tobacco plants and 3−4-week-old soybean plants. Control plants were infiltrated with 10 mM $MgCl_2$, while experimental plants were treated with *Pto*

https://doi.org/10.1021/acssensors.4c02645
ACS Sens. XXXX, XXX, XXX−XXX

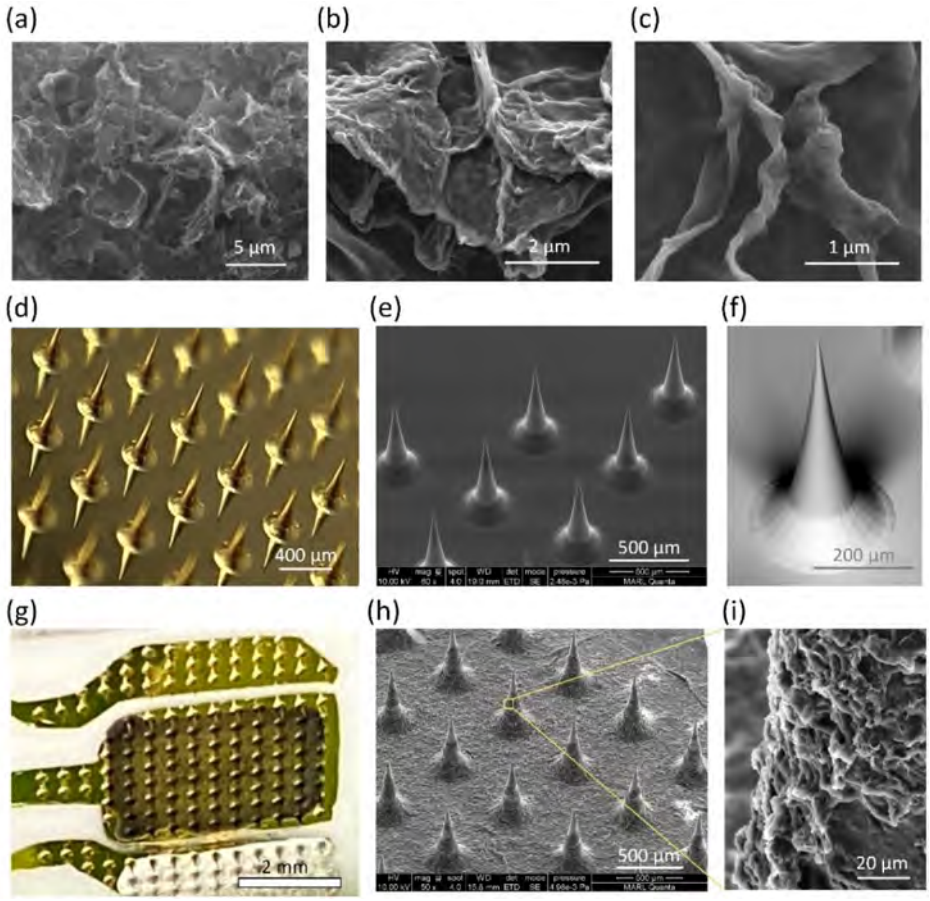

Figure 2. Morphology and structure of materials and components used in constructing a microneedle sensor with HRP/Cs-rGO biohydrogel. (a) SEM image of rGO with folded structures. (b) SEM image of Cs-rGO hydrogel. (c) SEM image of HRP/Cs-rGO biohydrogel. (d) Optical image of Au-coated microneedles. (e,f) SEM images of Au-coated microneedles. (g) Optical image of a fabricated microneedle sensor with HRP/Cs-rGO biohydrogel. (h,i) SEM images of microneedles functionalized with HRP/Cs-rGO biohydrogel.

DC3000 in 10 mM $MgCl_2$. Liquid samples were extracted from the leaves at 12 and 24 h after inoculation. Liquid samples were extracted from the collected leaves using a kitchen juice squeezer. For each sensor measurement, a 25 μL aliquot of the liquid sample extracted from the leaves was mixed with 25 μL of 10 mM PBS (pH 7.4) for soybean and 15 μL of PBS for tobacco. Subsequently, 30 μL of the mixed sample was pipetted onto the sensor surface to perform electrochemical detection of H_2O_2.

Quantitative Amplex Red Assay. To evaluate the accuracy of our sensors, we conducted a quantitative measurement of H_2O_2 concentration using the Amplex Red Assay, a fluorescence-based method in which H_2O_2 reacts with Amplex Red in the presence of HRP, producing the fluorescent resorufin. This assay was applied to measure H_2O_2 production in four mock-treated, and four *Pto* DC3000-inoculated tobacco leaves 12 h postinoculation. Samples preparation followed a previously established method,[47] except that 10 leaf discs (0.4 cm diameter) were collected per leaf, and 500 μL of 20 mM PBS (pH 6.5) was used per sample. The Amplex Red Assay kit (Invitrogen, Carlsbad, CA) was used according to the manufacturer's instructions. H_2O_2 levels were measured using a BioTek Synergy H1 microplate reader (Agilent Technologies, Santa Clara, CA) with an excitation wavelength of 540 nm and emission detection at 590 nm. H_2O_2 was quantified by a standard curve of known H_2O_2 concentrations as a function of fluorescence intensity.

RESULTS AND DISCUSSION

Material Characterization. The surface morphologies of rGO, Cs-rGO, and HRP/Cs-rGO biohydrogel were examined via scanning electron microscopy (SEM; FEI Quanta-FEG 250; Thermo Fisher Scientific, Waltham, MA). Figure 2a shows multiple layers with folded and agglomerated structures, resulting in the appearance of rGO nanosheets. The multilayered sheets of rGO likely arise from the stacking of layers.[42] Figure 2b displays the growth of the Cs-rGO hydrogel structure, which is due to the self-assembly of Cs and rGO nanosheets in an aqueous colloidal solution via hydrogen bonding and electrostatic interactions (Figure S1). Figure 2c illustrates the microstructures of the HRP/Cs-rGO biohydrogel, wherein the HRP enzyme is immobilized on the Cs-rGO surface by imine coupling between the $-NH_2$ groups of HRP enzyme and the $-NH_2$ groups of Cs-rGO via a GA cross-linker. This results in the formation of a porous network of HRP/Cs-rGO biohydrogel with a distinct surface morphology. Energy dispersive X-ray spectroscopy analysis (Figure S2) was conducted to investigate the surface elemental composition (C, N, and O) of the HRP/Cs-rGO biohydrogel. The weight percentages of C, N, and O in HRP/Cs-rGO were observed to be 70.03%, 11.36%, and 18.6%, respectively. Further, SEM studies were utilized to examine the surface morphologies of both the Au-coated bare microneedle array (Figure 2d-f) and the biohydrogel-coated microneedle array (Figure 2g). Figure 2h,i shows the biohydrogel coating on the surfaces of the needle and the base substrate of the sensor.

The X-ray diffraction (XRD; Siemens D500 X-ray diffractometer; Bruker Corporation; Billerica, MA) spectra of rGO (Figure S3a) exhibit a prominent peak at 2θ = 22.76°,

https://doi.org/10.1021/acssensors.4c02645
ACS Sens. XXXX, XXX, XXX−XXX

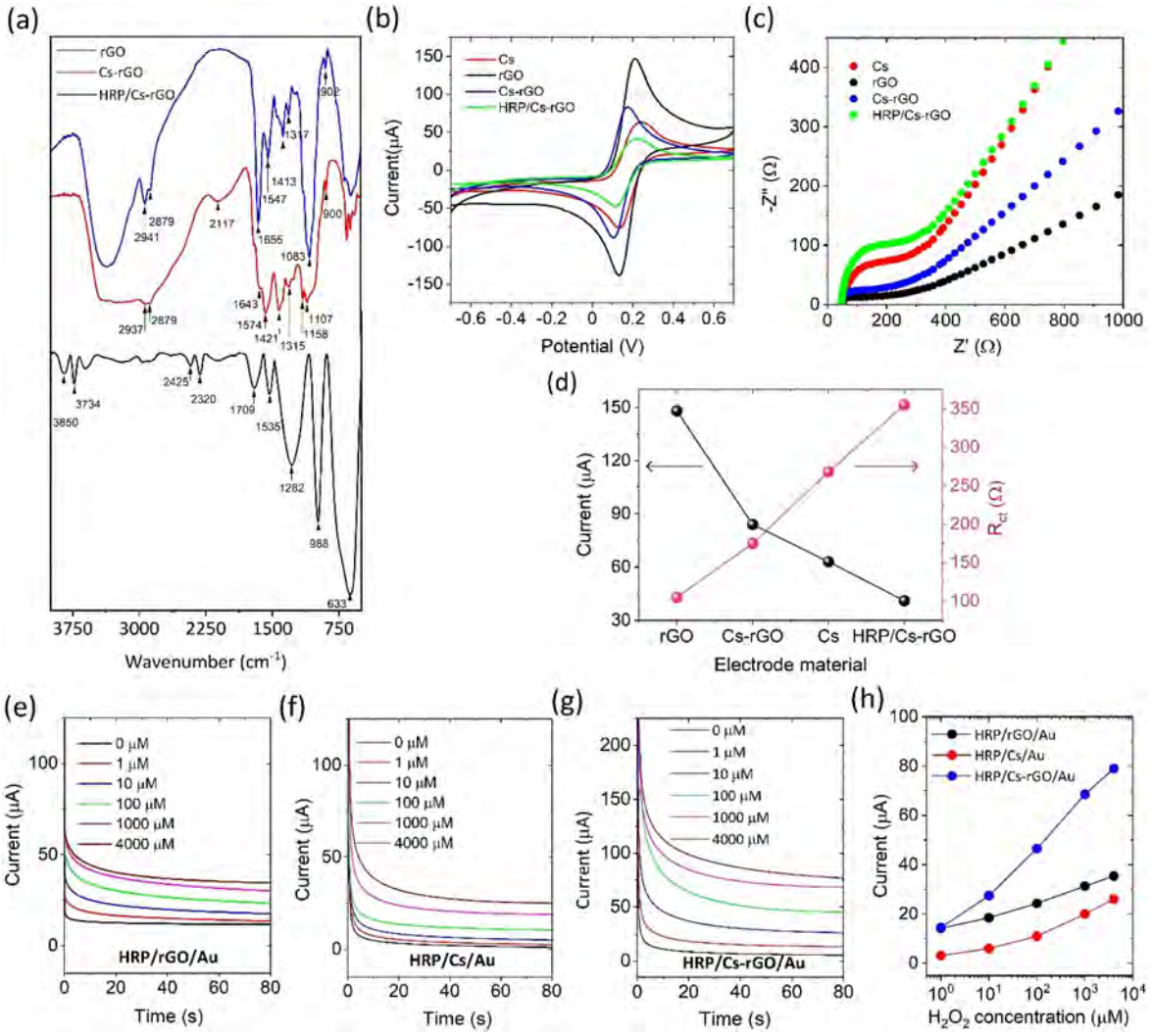

Figure 3. FTIR analysis of rGO, Cs-rGO, and HRP/Cs-rGO, along with the electrochemical properties of Au electrodes coated with these materials. (a) FTIR spectra of rGO, Cs-rGO, and HRP/Cs-rGO. (b,c) Electrochemical characterization of Cs, rGO, Cs-rGO, and HRP/Cs-rGO coated on an Au electrode surface in PBS (pH 7.4; 10 mM) containing 5 mM potassium ferro-ferricyanide, analyzed using CV (b) and EIS (c) techniques. (d) Comparison of anodic peak current and charge transfer resistance R_{ct} data for the Au electrode modified with Cs, rGO, Cs-rGO, and HRP/Cs-rGO. (e-g) CA responses of HRP/rGO/Au (e), HRP/Cs/Au (f), and HRP/Cs-rGO/Au (g) electrodes, in response to lab-prepared H_2O_2 samples with concentrations from 1 to 4000 μM. (h) Summary of CA current responses of the electrodes shown in (c–g) to varying H_2O_2 concentrations. The CA current values were recorded at 65 s from the respective CA response curves.

attributed to its (002) plane.[42] In the Raman spectrum of rGO (Figure S3b), acquired using a Renishaw inVia Raman spectrometer (Renishaw, Hoffman Estates, IL), the bands at 1354 and 1588 cm^{-1} correspond to the D and G bands, respectively. The D band indicates distortions due to specific defects, while the G band is associated with graphitic carbon.[42] Fourier transform infrared (FTIR; Bruker Tensor 37 FTIR spectrometer; Bruker Corporation; Billerica, MA) spectroscopy confirms the surface functionalization of rGO with Cs and the immobilization of the HRP enzyme on the Cs-rGO surface (Figure 3a). In rGO, the peak detected at 998 cm^{-1} is related to C−O stretching vibration, while the peak at 1282 cm^{-1} corresponds to C−H bending. The peaks at 1535 and 1709 cm^{-1} are associated with aromatic C═C and C═O stretching, respectively, and the peaks in the range of 2300−2450 cm^{-1} correspond to O−H vibration, indicating carboxylic groups in rGO.[48] For Cs-rGO, the peaks at 1107, 1158−1315, and 1421 cm^{-1} are associated with C−O−C stretching, −OH bending of alcohols, C−O stretching, and C−H bending vibrations of CH_2, respectively. The peaks at 1574 and 1639 cm^{-1} are related to −NH bending and C═O stretching, respectively, while the peaks at 2878 and 2939 cm^{-1} are due to C−H and N−H stretching, respectively, confirming the presence of Cs in the Cs-rGO matrix.[43,49,50] For HRP/Cs-rGO, two additional peaks at 1547 and 1655 cm^{-1} appear due to imine bonding between the HRP enzyme and Cs-rGO, indicating HRP enzyme immobilization on the Cs-rGO surface.[51]

Electrode Electrochemical Characterization. Cyclic voltammetry (CV) and electrochemical impedance spectroscopy (EIS) studies were performed using an electrochemical workstation (Model 1200C; CH Instrument; Austin, TX) to evaluate the electrochemical performance and interfacial properties of the prepared rGO, Cs, Cs-rGO, and HRP/Cs-rGO on an Au electrode surface (Figure 3b,c). The CV results showed that the Cs/Au electrode exhibited an anodic peak current of 62 μA, significantly lower than the rGO/Au electrode (148 μA) due to the higher resistance property of Cs. However, incorporating Cs with rGO increased the anodic

https://doi.org/10.1021/acssensors.4c02645
ACS Sens. XXXX, XXX, XXX−XXX

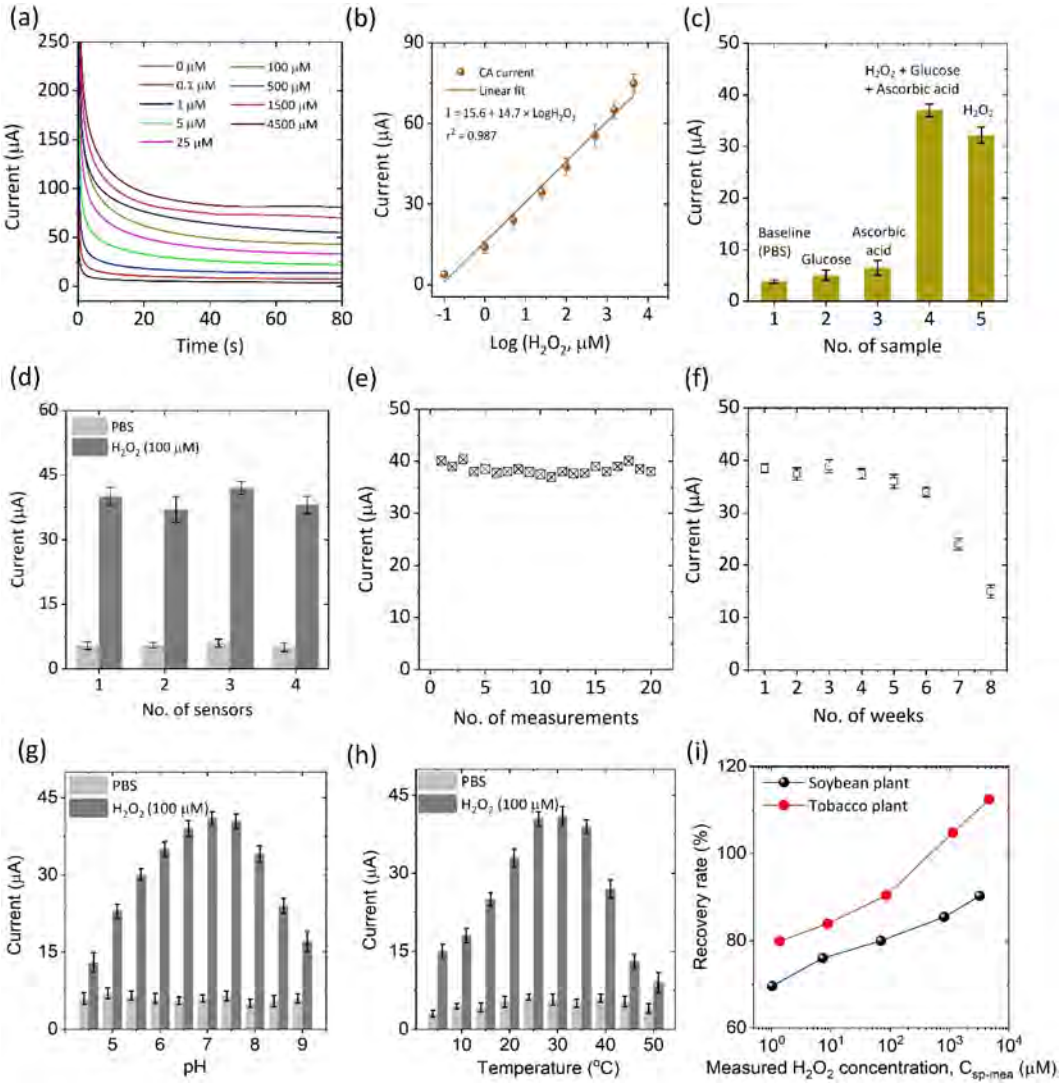

Figure 4. Sensor characterization. (a) CA response of the HRP/Cs-rGO microneedle sensor to varying concentrations of H_2O_2 up to 4500 μM in PBS (pH 7.4; 10 mM). (b) Calibration plot of the sensor, showing the CA current as a function of the log of the H_2O_2 concentration, recorded at 65 s from the CA response in (a). (c) Histogram comparing the CA response of the HRP/Cs-rGO/Au sensor to H_2O_2, glucose, ascorbic acid, and a combination of all three chemicals, each at 100 μM. (d) Reproducibility of the HRP/Cs-rGO/Au sensor, assessed by monitoring the CA response of four identical HRP/Cs-rGO/Au sensors to PBS and 100 μM H_2O_2. (e) Repeatability of the HRP/Cs-rGO/Au sensor, evaluated by repeatedly measuring the CA response to 100 μM H_2O_2. (f) Stability of the HRP/Cs-rGO/Au sensor, assessed by measuring the CA response to 100 μM H_2O_2 at regular intervals over an 8-week period. (g) Effect of pH on the CA response to 100 μM H_2O_2 in 10 mM PBS across a pH range of 4.5−9.0. (h) Effect of temperature on the CA response to 100 μM H_2O_2 over a temperature range of 5−50 °C. (i) Sensor recovery rate for H_2O_2 detection, measured by exposing the sensor to leaf extracts of mock-treated soybean and tobacco plants after the addition of known H_2O_2 concentrations.

peak current to 84 μA compared to the Cs/Au electrode alone, though it remained lower than the rGO/Au electrode. This was likely due to the formation of a cross-linked network between rGO and the −OH and $-NH_2$ groups of Cs. Upon the immobilization of HRP enzyme on the Cs-rGO surface, the redox current of the HRP/Cs-RGO/Au electrode further decreased to 41 μA. This reduction was attributed to the insulating nature of HRP enzyme and its macromolecular structure hindering electron transfer.

The EIS measurements (Figure 3c) for these electrodes aligned with the CV results. The Cs/Au electrode exhibited a charge transfer resistance (R_{ct}) of 268 Ω, higher than that of the rGO/Au electrode (105 Ω), due to decreased electrolyte ion mobility. The Cs-rGO/Au electrode had an intermediate R_{ct} value of 175 Ω, reflecting the combination of rGO and Cs properties. The HRP enzyme immobilization further increased the R_{ct} to 355 Ω, as the enzyme obstructed the charge transfer process of redox species. Figure 3d compares the anodic peak current and R_{ct} values of the different electrodes.

Notably, although the Cs-rGO/Au electrode exhibited a lower anodic peak current and a higher R_{ct} value than the rGO/Au electrode, the primary role of Cs was to enhance the CA current response of the HRP/Cs-rGO/Au electrode to H_2O_2. This enhancement likely resulted from increased HRP enzyme immobilization on the sensor surface, as demonstrated in our comparative experiments below. Without Cs, the HRP/rGO/Au electrode responded to H_2O_2 concentrations (Figure 3e), but the response increase was minimal at low H_2O_2 concentrations (1−10 μM) and became significant only at higher concentrations (10−4000 μM). Similarly, without rGO,

https://doi.org/10.1021/acssensors.4c02645
ACS Sens. XXXX, XXX, XXX−XXX

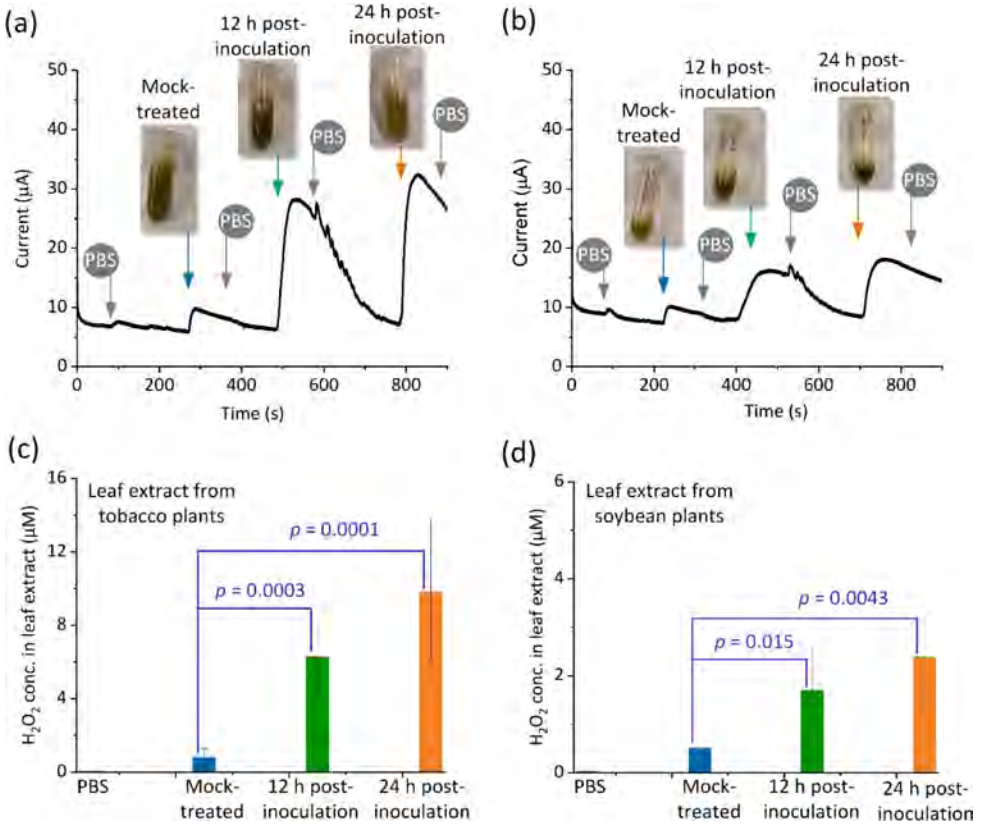

Figure 5. Measurement of H_2O_2 concentration in leaf extracts using the sensor. (a,b) CA response of the HRP/Cs-rGO/Au sensor to leaf extracts from mock-treated and *Pto* DC3000-inoculated tobacco (a) and soybean (b) plants at 12- and 24-h postinoculation. The sensor surface was washed with PBS between loading different leaf extract samples. (c,d) Converted H_2O_2 concentrations in leaf extracts from mock-treated and *Pto* DC3000-inoculated tobacco plants at 12- and 24-h postinoculation. Error bars represent standard deviations from H_2O_2 measurements for the leaf extracts from five plants.

the HRP/Cs/Au electrode exhibited a comparable response pattern to the HRP/rGO/Au electrode (Figure 3f), though with lower current levels. In contrast, the HRP/Cs-rGO/Au electrode, incorporating both Cs and rGO, displayed a significantly higher response current across the same concentration range (Figure 3g). While direct quantification of immobilized HRP enzyme on these electrodes is challenging, the results in Figure 3h indicate that the combination of Cs and rGO enhanced the sensor response to H_2O_2, likely by increasing enzyme loading on the Cs-rGO/Au electrode.[52]

Sensor Characterization Using Standard H_2O_2 Samples. The sensor was tested to perform the electrochemical detection of H_2O_2 using the chronoamperometry (CA) technique. The CA method measured the current changes at an applied potential of 0.5 V between the WE and CE. The sensor surface was exposed successively to standard H_2O_2 solutions at various concentrations up to 4500 μM (Figure 4a). The CA current increased with increasing H_2O_2 concentration due to the enzymatic catalytic reaction of HRP with H_2O_2.[53] To calibrate the sensor, CA current values were recorded at 65 s for all concentrations of H_2O_2. The calibration plot of the sensor (Figure 4b) demonstrates a linear relationship between the CA current and the logarithm of the H_2O_2 concentration, described by eq 1:

$$I\ (\mu A) = 15.6\ (\mu A) + 14.7\ (\mu A/\mu M) \times \mathrm{Log}\, H_2O_2\ (\mu M), \quad r^2 = 0.987 \tag{1}$$

The limit of detection (*LoD*) of the sensor was determined to be 0.06 μM using the equation LoD = 3 × SD/m,[54] where SD is the standard deviation of the CA current for the blank solution from three repeated measurements, and m is the slope of the linear regression.

The specificity of the sensor was evaluated by testing 100 μM of H_2O_2 in the presence of representative interfering molecules, namely, glucose and ascorbic acid, each at a concentration of 100 μM (Figure 4c). The baseline CA response of the sensor was established at 5 μA using PBS. Upon exposed to 100 μM of H_2O_2 without interfering molecules, the CA response increased to 33 μA. In the solution containing H_2O_2, glucose, and ascorbic acid, there was no statistically significant change in the sensor's output signal compared to its response to H_2O_2 alone (p = 0.1, which is greater than the significance level of 0.05; p value calculated via two-sample t test). Exposure to glucose and ascorbic acid in the absence of H_2O_2 resulted in CA current of 7.5 μA and 6.0 μA, respectively, further indicating high specificity of the sensor.

The sensor demonstrated considerable reproducibility, repeatability, and stability. Reproducibility was assessed by exposing four similar sensors to 100 μM of H_2O_2. The resulting current responses (Figure 4d) showed substantial reproducibility, with a low relative standard deviation (RSD) value of 5.3%. Repeatability was evaluated by measuring the CA response over 20 repeated measurements, each lasting 65 s (Figure 4e). After each measurement, the sensor was washed

https://doi.org/10.1021/acssensors.4c02645
ACS Sens. XXXX, XXX, XXX−XXX

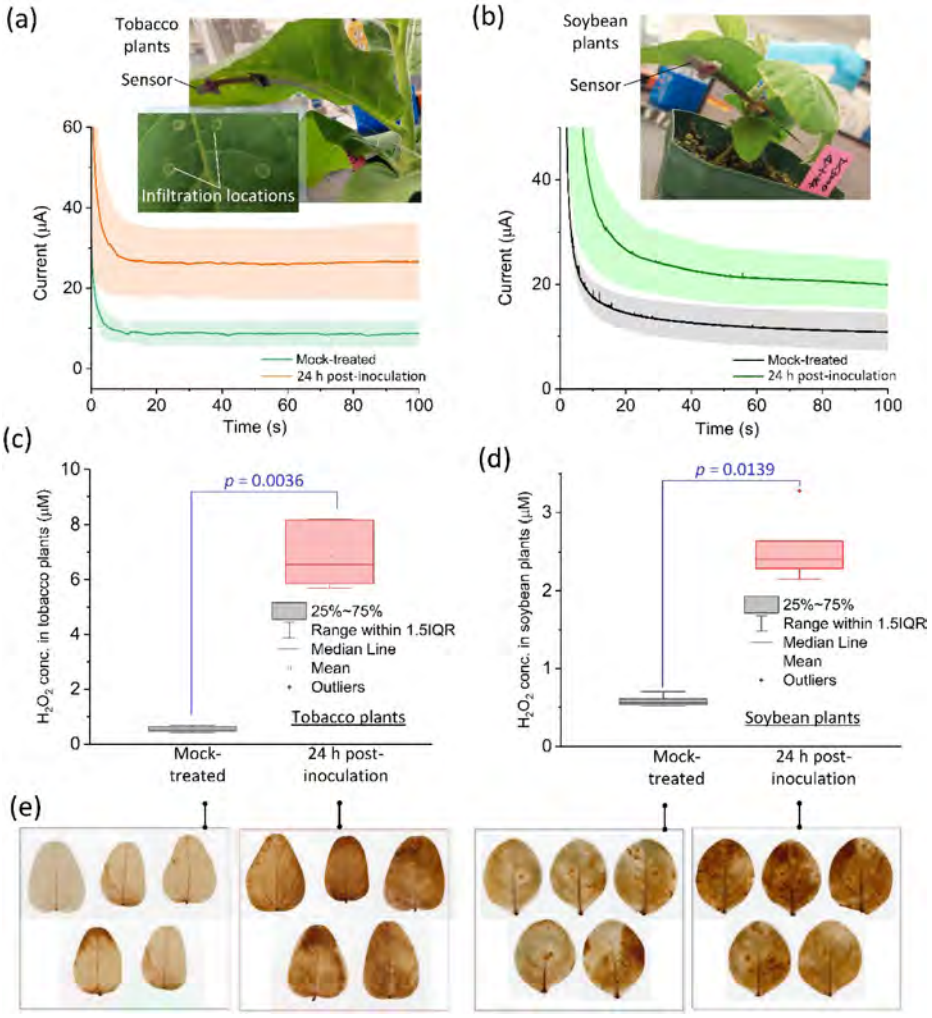

Figure 6. In situ detection of H_2O_2 using the microneedle sensor. (a,b) CA response of the HRP/Cs-rGO/Au sensors attached to the back of leaves from mock-treated and *Pto* DC3000-inoculated tobacco (a) and soybean (b) plants for in situ H_2O_2 measurement. The shaded areas in each panel represent the standard deviation of measurements taken from 15 mock-treated and 25 inoculated plants. (c,d) Sensor-measured H_2O_2 concentrations in tobacco (c) and soybean (d) plants corresponding to the CA response data in (a) and (b), respectively. (e) Conventional DAB staining for colorimetric monitoring of H_2O_2 production in soybean and tobacco leaves in the mock plants and Inoculated plants 24 h postinoculation with *Pto* DC3000 pathogen. For each plant type, 5 mock-treated and 5 Inoculated leaves were analyzed.

with PBS. The sensor displayed a consistent CA current response, with a small reduction in CA current observed after 20 consecutive measurements, resulting in an RSD (N = 3) of 7.3%. Stability was evaluated over 8 weeks at 25 °C by measuring the CA response for 100 μM of H_2O_2 once a week (Figure 4f). After each measurement, the sensor was washed with PBS and stored at 4 °C. The sensor displayed a relatively stable CA current response, with a significant reduction observed after 6 weeks, resulting in an RSD (N = 3) of less than 10%.

Next, the effect of pH on the sensing performance of the HRP/Cs-rGO/Au sensor was evaluated by measuring its CA response to 100 μM H_2O_2 in 10 mM PBS across a pH of 4.5−9.0 (Figure 4g). The sensor exhibited high current responses between pH 6.5 and 7.4, with a decline observed below pH 6.5 and above pH 8.0. This trend aligned with the optimal activity range of HRP (6.5−7.5).[55,56] Consequently, PBS (pH 7.4) was selected for further experiments for high soluble peroxidase activity at this pH. Notably, in the absence of H_2O_2, the background signal remained low across different pH levels.

Additionally, the impact of temperature on the catalytic reaction between H_2O_2 and HRP on the sensor surface was investigated (Figure 4h). The sensor was exposed to 100 μM H_2O_2 in 10 mM PBS (pH 7.4) at temperatures ranging from 5 to 50 °C. The CA current initially increased with rising temperature, reaching high response levels from 25 to 35 °C, and peaking at 30 °C due to enhanced HRP catalytic activity. However, at higher temperatures, the current decreased, likely due to structural damage to HRP impairing its function.[57] Importantly, in the absence of H_2O_2, the sensor exhibited a minimal response to temperature variations, maintaining a nearly constant background current.

Furthermore, the recovery rate of the sensor was evaluated using leaf extract from mock-treated tobacco and soybean plants, spiked with known H_2O_2 concentrations ranging from 1 to 4000 μM. The CA responses of the sensors were recorded (Figure S5), and the H_2O_2 concentrations in the spiked samples were measured (Figure 4i). The recovery rate (%) was calculated using eq 2:[58]

https://doi.org/10.1021/acssensors.4c02645
ACS Sens. XXXX, XXX, XXX−XXX

$$\text{Recovery Rate}\ (\%) = (C_{\text{sp-mea}} - C_{\text{unsp-mea}})/C_{\text{sp-add}} \times 100 \quad (2)$$

where $C_{\text{sp-mea}}$ is the measured H_2O_2 concentration in spiked samples, $C_{\text{unsp-mea}}$ is the baseline H_2O_2 concentration in unspiked samples, and $C_{\text{sp-add}}$ is the known H_2O_2 concentration added for spiking. As shown in Figure 4i, the recovery rates ranged from 70−90% in soybean leaf extract and 80−110% in tobacco leaf extract. The recovery rate increased with higher H_2O_2 concentrations in both plant extracts.

Detection of H_2O_2 in Leaf Extracts. The sensor demonstrated its analytical capability by detecting H_2O_2 in leaf extracts from tobacco and soybean plants. Initially, PBS was pipetted onto the sensor surface to establish the baseline. Then, a mixed solution of PBS and leaf extract from either a mock-treated plant, a *Pto* DC3000-inoculated tobacco plant 12 h postinoculation, or a *Pto* DC3000-inoculated tobacco plant 24 h postinoculation was sequentially applied to the sensor surface to detect H_2O_2 concentrations. Before applying a new sample, the CA response of the sensor was recorded, and the sensor surface was rinsed with PBS (Figure 5). The sensor showed a minor increase in CA current (∼9 μA) for the mock-treated tobacco plant compared to the baseline current (∼6 μA) due to its low H_2O_2 level. In contrast, *Pto* DC3000-inoculated tobacco plants 12 and 24 h postinoculation exhibited a significant increase in CA current to ∼27 μA and ∼31.6 μA, respectively (Figure 5a) due to higher H_2O_2 levels.

Similarly, for soybean plants, the sensor measurement was conducted on a mixture of PBS and leaf extract from either a mock-treated plant or a *Pto* DC3000-inoculated plant (12 or 24 h postinoculation) (Figure 5b). The result showed that H_2O_2 concentrations became elevated in *Pto* DC3000-inoculated soybean leaves, evidenced by a small increase in CA current (∼9.4 μA) for the mock-treated plant, compared to a distinct increase in current for the plants at 12 h (∼16 μA) and 24 h postinoculation (∼19 μA) (Figure 5b).

Figure 5c,d illustrates the measured H_2O_2 concentrations in the leaf extracts from mock-treated and *Pto* DC3000-inoculated tobacco (Figure 5c) and soybean (Figure 5d) plants at 12- and 24-h postinoculation. The concentrations were obtained by applying CA currents to the calibration given in eq 1. For tobacco plants, the H_2O_2 concentrations in the mock-treated, 12-h postinoculation, 24-h postinoculation samples were 0.9 ± 0.3 μM, 6.3 ± 1.6 μM, and 10.7 ± 2.2 μM, respectively. In soybean plants, the corresponding values were 0.56 ± 0.07 μM, 1.4 ± 0.4 μM, and 2.1 ± 0.6 μM, respectively. Significant plant-to-plant variation in H_2O_2 levels was observed within the same species under the same treatment, as reflected by the large standard deviation for the data in Figure 5c,d. Despite this variability, a significant difference in H_2O_2 production was evident between the inoculated and mock-treated plants. Statistical analysis using a *t* test confirmed a significant increase in sensor output for *Pto* DC3000-inoculated samples at 12 h compared to the mock-treated samples (p = 0.0003 for tobacco; p = 0.015 for soybean) and 24 h (p = 0.0001 for tobacco; p = 0.0043 for soybean).

These results demonstrated the ability of the sensor to distinguish the defense response experienced by the plants and quantify H_2O_2 concentrations. The only required sample preparation for using this sensor to detect H_2O_2 in leaf extracts was to squeeze liquid from leaves and mix it with a PBS solution, making field implementation possible. The total time required to complete one measurement, including sample preparation (taking about 2 min) and H_2O_2 detection using the sensor (taking about 1 min), was approximately 3 min.

In Situ H_2O_2 Measurement in Plant Leaves. For in situ H_2O_2 measurement, microneedle sensors were attached to the back of tobacco and soybean leaves. The experiment involved 6−8 week-old tobacco plants and 3−4 week-old soybean plants, which included both mock-treated and *Pto* DC3000-inoculated groups. CA current values from the attached sensors were recorded at 65 s after attachment.

For tobacco plants (Figure 6a), the sensors exhibited a distinct increase in CA current, reaching 28.2 ± 7.6 μA in inoculated plants, compared to 11 ± 4.1 μA in mock-treated plants, indicating higher H_2O_2 levels in inoculated tobacco plants (Figure 6a). Using the calibration from eq 1, the H_2O_2 concentrations were determined to be 6.9 ± 1.1 μM in inoculated plants and 0.56 ± 0.2 μM in mock-treated plants (Figure 6c). Despite all plants being at the same 24-h postinoculation stage, substantial variations in H_2O_2 production were observed among the tobacco plants, due to large plant-to-plant variations. A *t* test revealed a statistically significant difference in the sensor output for *Pto* DC3000-inoculated plants compared to the mock-treated plants (p = 0.0036).

When attached to the soybean leaves, the sensors (Figure 6b) produced higher CA current values representing higher H_2O_2 concentrations in the inoculated plants (21 ± 5 μA; corresponding to 2.6 ± 0.4 μM) compared to the mock-treated plants (11.7 ± 3.5 μA; corresponding to 0.58 ± 0.1 μM) (Figure 6d). However, significant plant-to-plant variations in both CA current and H_2O_2 concentration were also present in this in situ measurement for soybean plants. A *t* test confirmed a statistically significant difference in sensor output between *Pto* DC3000-inoculated and mock-treated soybean plants (p = 0.0139).

The demonstrated in situ measurement highlighted the microneedle sensor as a promising alternative for H_2O_2 detection. The total time required for direct in situ measurement was approximately 1 min from sensor insertion to data production. Therefore, the sensor showed great potential as a portable tool for rapid in situ H_2O_2 measurement for plant tissues, eliminating the need for sample preparation.

Comparing Sensor Measurement with Qualitative DAB Staining. To compare and evaluate the effectiveness of our sensor in detecting H_2O_2 production in plants, soybean and tobacco leaves were inoculated with *Pto* DC3000 bacteria, and DAB staining was employed to detect the presence of H_2O_2 and peroxidase activity in tissue samples. In general, DAB serves as a chromogenic substrate that is oxidized to produce a brown precipitate in the presence of H_2O_2 and peroxidase enzyme, indicating the presence and localization of H_2O_2 in the leaf samples.[59] As shown in Figure 6e, no substantial accumulation of H_2O_2 was observed in soybean and tobacco leaves 24 h after treatment with $MgCl_2$. In contrast, at 24 h after pathogen inoculation, a substantial amount of H_2O_2-induced brown precipitate was observed throughout the leaves of soybean and tobacco (Figure 6e). The results obtained with the sensor (Figure 6a−d) were consistent with those obtained by conventional DAB staining, demonstrating the performance of the sensor in detecting H_2O_2. More importantly, the sensor method overcomes the limitations of DAB staining by allowing for the quantitative determination of H_2O_2. Therefore, this

https://doi.org/10.1021/acssensors.4c02645
ACS Sens. XXXX, XXX, XXX−XXX

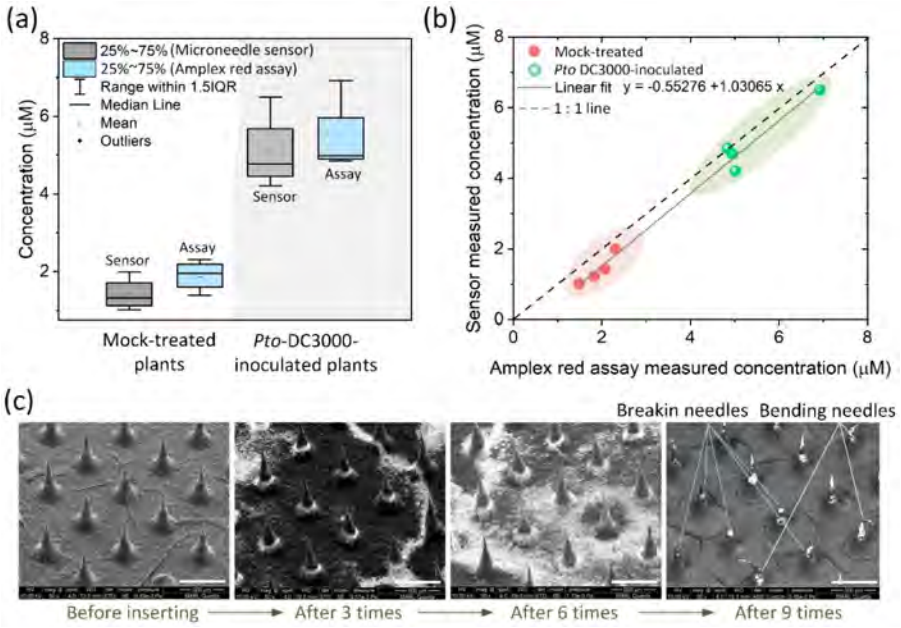

Figure 7. In situ detection of H_2O_2 using the microneedle sensor. (a) Box plot comparison of H_2O_2 concentrations measured by the microneedle sensor and the Amplex Red Assay in mock-treated and Pto DC3000-inoculated tobacco plants. (b) Correlation between H_2O_2 concentrations measured by the microneedle sensor and the Amplex Red Assay, with a linear regression line showing a slight underestimation by the sensor compared to the assay. The 1:1 reference line is included for comparison. (c) SEM images showing the structure of the microneedles before insertion and after 3, 6, and 9 insertions into tobacco leaves.

Table 1. Comparative Assessment of HRP/Cs-rGO/Au Sensor Features in Comparison with Other H_2O_2 Electrochemical Sensors Reported in the Literature[a]

Bioelectrode material	Measurement technique	Detection range (μM)	LoD (μM)	Sensitivity	Response time	In situ measurement
MWCNT-Ti_3C_2Tx-Pd/GCE[23]	Amperometry	50−18,000	3.83	293.85 μA/mM cm^2	NA	No
Au nanodots-ITO[26]	Differential pulse voltammetry	0−1000	1.0	NA	NA	No
Au nanodots/SS electrode[28]	Amperometry	10−1000	3.97	NA	2.3 s	Yes
Co_3O_4/MWCNTs/gelatin/HRP/GCE[63]	Amperometry	0.74−19	0.7	NA	5 s	No
Au-SPAN/HRP/GCE[64]	Amperometry	10−2000	1.6	NA	NA	No
Nafion/HRP/3D-Bi_2WO_6/GCE[65]	Amperometry	0.5−250	0.18	NA	NA	No
HRP/TB/CCB[66]	Cyclic voltammetry	0.429−455	0.17	0.071 μA/μM	2 s	No
Ag NPs/3DG[67]	Amperometry	30−16,210	14.9	1.09 mA/mM cm^2	NA	No
Hb/SWCNTs/CFUMEs[68]	Amperometry	4.90−405	4	1.07 log(A)/ log(M) cm^2	NA	No
HRP/Cs-rGO (this work)	Chronoamperometry	0.1−4500	0.06	14.7 μA/μM	65 s	Yes

[a]MWCNT: multiwalled carbon nanotube; Ti_3C_2Tx-Pd: titanium carbide−palladium; GCE: glassy carbon electrode; SS: stainless steel; HRP: horseradish peroxidase; SPAN: self-doped polyaniline nanofibers; Bi_2WO_6: bismuth tungstate; TB: toluidine blue; CCB: ceramic composite biosensor; Hb: hemoglobin; CFUME: carbon fiber ultramicroelectrode; Cs: chitosan; NA: not available.

sensor provides a simple, rapid, and quantitative means of monitoring H_2O_2 production in plants.

Comparing Sensor Measurement with Quantitative Amplex Red Assay. We further assessed the accuracy of our microneedle sensors by quantifying H_2O_2 levels using the Amplex Red Assay and comparing the results with sensor measurements. As detailed in the Experimental Section, this fluorescence-based assay was used to measure H_2O_2 production in mock-treated and *Pto* DC3000-inoculated tobacco plants. For in situ measurements, our microneedle sensors were attached to the leaves of the same plants.

The Amplex Red Assay detected H_2O_2 concentrations of 5.43 ± 0.99 μM in inoculated plants and 1.92 ± 0.35 μM in mock-treated plants (Figure 7a), while our sensors measured corresponding concentrations of 5.06 ± 0.99 μM and 1.41 ± 0.42 μM, respectively. Notably, the linear regression of sensor-measured values against assay-measured values falls below the 1:1 ratio line, indicating that the Amplex Red Assay slightly overestimated H_2O_2 levels (Figure 7b). This overestimation was expected due to the susceptibility of the assay to background autofluorescence artifacts in tobacco.[60] Despite this, the close agreement between the two methods validates the accuracy of our sensors while highlighting their advantage in mitigating autofluorescence interference.

This advantage becomes even more pronounced when testing plants with high autofluorescence. In our case, soybean exhibited excessive autofluorescence approximately 2 orders of magnitude higher than the H_2O_2-triggered fluorescence signals, severely obscuring the H_2O_2-induced fluorescence response and compromising its reliability. In contrast, our sensor-based approach circumvents these limitations while also eliminating

https://doi.org/10.1021/acssensors.4c02645
ACS Sens. XXXX, XXX, XXX−XXX

the need for specialized equipment and labor-intensive procedures required by the Amplex Red Assay.

Although our plant sensor was designed for single-use H_2O_2 detection, we conducted insertion experiments to evaluate its durability by assessing its structural integrity before and after insertion into tobacco and soybean leaves. The results demonstrated that the microneedles reliably punctured the leaves without any risk of buckling or breaking, even after six insertions (Figure 7c). However, after nine insertions, both microneedle bending and breakage were observed, with similar results seen in soybean leaves. This is not a concern, as the sensor is primarily intended for disposable measurement applications. The relatively high durability of the needles is attributed to the mechanical properties of polyurethane, the primary needle material, which has a significantly higher Young's modulus (179.3 MPa)[61] compared to soft leaves (e.g., tobacco leaf: 3.5 MPa)[62] making the microneedles much more rigid and resistant to deformation. Additionally, the tensile strength of polyurethane (45.86 MPa)[61] far exceeds that of the tobacco leaf (0.57 MPa),[62] ensuring that the leaf will tear or break under force long before the microneedles are at risk of damage.

CONCLUSION

In conclusion, we have developed a microneedle plant sensor for the rapid assessment of H_2O_2 levels in tobacco and soybean plants under biotically stressed and unstressed conditions. This sensor technology offers a portable, on-site solution for H_2O_2 measurement, eliminating the need for the intricate and time-consuming sample preparation required by conventional methods such as histological staining. The sensor demonstrated rapid detection capabilities, with a response time of around one minute for in situ measurements. Additionally, this sensor exhibited significant sensitivity (14.7 μA/μM), a low LOD (0.06 μM), a wide dynamic range (0.1−4500 μM), and high portability, outperforming other H_2O_2 electrochemical sensors in the literature (Table 1). The technology features H_2O_2-specific microneedles functionalized with a hydrogel composed of natural biopolymer, rGO, and HRP enzyme, which together provide biocompatibility, high electrochemical properties, and a high enzyme loading capacity. The changes in H_2O_2 levels under pathogen stress, monitored by this sensor, were compared to conventional histological staining methods, demonstrating the capability of the sensor for in situ measurement.

Furthermore, this sensor technology could be refined by integrating biohydrogel with various enzyme molecules specific to other ROS, such as hyperoxide/superoxide, hydroxyl radical, alkoxy radical, and hypochlorite anion. Additionally, investigating the integration of this sensor with other plant sensors on a single sensing patch could enable multimodality detection, providing a better understanding of plant responses to various stresses. Incorporating various plant sensors[69−72] with soil and environmental sensors[73−77] into a wireless communication network[78] would enable real-time monitoring. This integration would facilitate more effective management of diseases, nutrients, and water. Ultimately, it would contribute to the early detection and management of various biotic and abiotic stresses in plants, significantly enhancing crop health and productivity.

ASSOCIATED CONTENT

Supporting Information

The Supporting Information is available free of charge at https://pubs.acs.org/doi/10.1021/acssensors.4c02645.

Schematic illustration of the key synthesis steps for the HRP/Cs-rGO biohydrogel; EDS spectrum of HRP/Cs-rGO, along with the quantitative composition of the HRP/Cs-rGO biohydrogel; XRD and Raman spectra of rGO; optimization of Cs and rGO weight percentage in HRP/Cs-rGO biohydrogel; CA responses recorded during studying recovery rate (PDF)

AUTHOR INFORMATION

Corresponding Author

Liang Dong − *Department of Electrical and Computer Engineering, Iowa State University, Ames, Iowa 50011, United States; Microelectronics Research Center, Iowa State University, Ames, Iowa 50011, United States;* orcid.org/0000-0002-0967-4955; Phone: + 1 (515) 294-0388; Email: ldong@iastate.edu

Authors

Nawab Singh − *Department of Electrical and Computer Engineering, Iowa State University, Ames, Iowa 50011, United States; Microelectronics Research Center, Iowa State University, Ames, Iowa 50011, United States*

Qinming Zhang − *Department of Electrical and Computer Engineering, Iowa State University, Ames, Iowa 50011, United States; Microelectronics Research Center, Iowa State University, Ames, Iowa 50011, United States*

Weihui Xu − *Department of Plant Pathology, Entomology, and Microbiology, Iowa State University, Ames, Iowa 50011, United States*

Steven A. Whitham − *Department of Plant Pathology, Entomology, and Microbiology, Iowa State University, Ames, Iowa 50011, United States*

Complete contact information is available at: https://pubs.acs.org/10.1021/acssensors.4c02645

Author Contributions

N.S. designed and conducted the experiments. N.S. fabricated the sensing materials and devices. Q.Z. assisted in device fabrication. W.X. prepared plant and bacterial samples and conducted DAB staining tests. L.D. conceived the sensor concept. L.D. and S.A.W. supervised the research of N.S., Q.Z., and W.X. All authors analyzed data. N.S., W.X., and L.D. drafted the manuscript. S.A.W. provided input to the draft.

Notes

The authors declare no competing financial interest.

ACKNOWLEDGMENTS

This work was supported in part by the Iowa Soybean Research Center and the Plant Sciences Institute at Iowa State University; in part by the U.S. Department of Agriculture—National Institute of Food and Agriculture (USDA-NIFA) under grant numbers 2020-67021-31528, 2020-68013-30934, and Hatch Project 04308; in part by the U.S. National Science Foundation under grant number CNS-2125484; in part by the AI Research Institutes program supported by NSF and USDA-NIFA under the AI Institute for Resilient Agriculture under grant number 2021-67021-35329.

REFERENCES

(1) Chakraborty, S.; Newton, A. C. Climate change, plant diseases and food security: An overview. *Plant Pathol.* **2011**, *60* (1), 2−14.

(2) Zandalinas, S. I.; Fritschi, F. B.; Mittler, R. Global warming, climate change, and environmental pollution: Recipe for a multifactorial stress combination disaster. *Trends Plant Sci.* **2021**, *26* (6), 588−599.

(3) Yan, Y.; Ni, M.; Wang, F.; Yu, Y.; Gong, X.; Huang, Y.; Wang, F.; Li, C.; Wang, F. Metal−Organic Framework-Based Biosensor for Detecting Hydrogen Peroxide in Plants through Color-to-Thermal Signal Conversion. *ACS Nano* **2022**, *16* (9), 15175−15187.

(4) Jetz, W.; Cavender-Bares, J.; Pavlick, R.; Schimel, D.; Davis, F. W.; Asner, G. P.; Ustin, S. L.; Kattge, J.; Latimer, A. M.; Moorcroft, P.; Schaepman, M. E. Monitoring plant functional diversity from space. *Nat. Plants* **2016**, *2* (3), 1−5.

(5) Roper, J. M.; Garcia, J. F.; Tsutsui, H. Emerging technologies for monitoring plant health in vivo. *ACS Omega* **2021**, *6* (8), 5101−5107.

(6) Ali, M. A.; Dong, L.; Dhau, J.; Khosla, A.; Kaushik, A. Perspective—electrochemical sensors for soil quality assessment. *J. Electrochem. Soc.* **2020**, *167* (3), 037550.

(7) Nehra, M.; Dilbaghi, N.; Marrazza, G.; Kaushik, A.; Sonne, C.; Kim, K. H.; Kumar, S. Emerging nanobiotechnology in agriculture for the management of pesticide residues. *J. Hazard. Mater.* **2021**, *401*, 123369.

(8) Mittler, R.; Vanderauwera, S.; Suzuki, N.; Miller, G. A. D.; Tognetti, V. B.; Vandepoele, K.; Van Breusegem, F.; Shulaev, V.; Van Breusegem, F. ROS signaling: The new wave? *Trends Plant Sci.* **2011**, *16* (6), 300−309.

(9) Choudhury, F. K.; Rivero, R. M.; Blumwald, E.; Mittler, R. Reactive oxygen species, abiotic stress and stress combination. *Plant J.* **2017**, *90* (5), 856−867.

(10) Miller, G.; Schlauch, K.; Tam, R.; Cortes, D.; Torres, M. A.; Shulaev, V.; Mittler, R.; Mittler, R. The plant NADPH oxidase RBOHD mediates rapid systemic signaling in response to diverse stimuli. *Sci. Signaling* **2009**, *2* (84), ra45−ra45.

(11) Niemeyer, J.; Scheuring, D.; Oestreicher, J.; Morgan, B.; Schroda, M. Real-time monitoring of subcellular H_2O_2 distribution in Chlamydomonas reinhardtii. *Plant Cell* **2021**, *33* (9), 2935−2949.

(12) Lew, T. T. S.; Koman, V. B.; Silmore, K. S.; Seo, J. S.; Gordiichuk, P.; Kwak, S. Y.; Strano, M. S.; Ang, M. C.-Y.; Khong, D. T.; Lee, M. A.; Chan-Park, M. B. Real-time detection of wound-induced H_2O_2 signalling waves in plants with optical nanosensors. *Nat. Plants* **2020**, *6* (4), 404−415.

(13) Zulfugarov, I. S.; Tovuu, A.; Kim, J. H.; Lee, C. H. Detection of reactive oxygen species in higher plants. *J. Plant. Biol.* **2011**, *54*, 351−357.

(14) Ortega-Villasante, C.; Burén, S.; Barón-Sola, Á.; Martínez, F.; Hernández, L. E. In vivo ROS and redox potential fluorescent detection in plants: Present approaches and future perspectives. *Methods* **2016**, *109*, 92−104.

(15) Olson, P. D.; Varner, J. E. Hydrogen peroxide and lignification. *Plant J.* **1993**, *4* (5), 887−892.

(16) Fernando, C. D.; Soysa, P. Optimized enzymatic colorimetric assay for determination of hydrogen peroxide (H_2O_2) scavenging activity of plant extracts. *MethodsX* **2015**, *2*, 283−291.

(17) Perez, F. J.; Rubio, S. An improved chemiluminescence method for hydrogen peroxide determination in plant tissues. *Plant Growth Regul.* **2006**, *48*, 89−95.

(18) Kwak, S. Y.; Wong, M. H.; Lew, T. T. S.; Bisker, G.; Lee, M. A.; Kaplan, A.; Strano, M. S.; Liu, A. T.; Koman, V. B.; Sinclair, R.; Hamann, C. Nanosensor technology applied to living plant systems. *Annu. Rev. Anal Chem.* **2017**, *10* (1), 113−140.

(19) Shaw, D. S.; Honeychurch, K. C. Nanosensor applications in plant science. *Biosensors* **2022**, *12* (9), 675.

(20) Lee, G.; Wei, Q.; Zhu, Y. Emerging wearable sensors for plant health monitoring. *Adv. Funct. Mater.* **2021**, *31* (52), 2106475.

(21) Wu, H.; Nißler, R.; Morris, V.; Herrmann, N.; Hu, P.; Jeon, S. J.; Giraldo, J. P.; Giraldo, J. P. Monitoring plant health with near-infrared fluorescent H_2O_2 nanosensors. *Nano Lett.* **2020**, *20* (4), 2432−2442.

(22) Giraldo, J. P.; Landry, M. P.; Kwak, S. Y.; Jain, R. M.; Wong, M. H.; Iverson, N. M.; Strano, M. S.; Strano, M. S. A ratiometric sensor using single chirality near-infrared fluorescent carbon nanotubes: Application to in vivo monitoring. *Small* **2015**, *11* (32), 3973−3984.

(23) Zhang, J.; Lu, M.; Zhou, H.; Du, X.; Du, X. Assessment of salt stress to arabidopsis based on the detection of hydrogen peroxide released by leaves using an electrochemical sensor. *Int. J. Mol. Sci.* **2022**, *23* (20), 12502.

(24) Wang, J.; Wang, L.; Di, J.; Tu, Y. Electrodeposition of gold nanoparticles on indium/tin oxide electrode for fabrication of a disposable hydrogen peroxide biosensor. *Talanta* **2009**, *77* (4), 1454−1459.

(25) Lima, A. S.; Prieto, K. R.; Santos, C. S.; Valerio, H. P.; Garcia-Ochoa, E. Y.; Huerta-Robles, A.; Bertotti, M.; Di Mascio, P.; Bertotti, M. In-vivo electrochemical monitoring of H_2O_2 production induced by root-inoculated endophytic bacteria in Agave tequilana leaves. *Biosens. Bioelectron.* **2018**, *99*, 108−114.

(26) Sun, L.; Pan, Y.; Wu, J.; Zhao, D.; Hui, M.; Zhu, S.; Zhang, C.; Li, D.; Song, F.; Zhang, C. Paper-based analytical devices for the rapid and direct electrochemical detection of hydrogen peroxide in tomato leaves inoculated with Botrytis cinerea. *Sensors* **2020**, *20* (19), 5512.

(27) Parrilla, M.; Sena-Torralba, A.; Steijlen, A.; Morais, S.; Maquieira, Á.; De Wael, K. A 3D-printed hollow microneedle-based electrochemical sensing device for in situ plant health monitoring. *Biosens. Bioelectron.* **2024**, *251*, 116131.

(28) Huo, D.; Li, D.; Xu, S.; Tang, Y.; Xie, X.; Li, D.; Sun, L.; Zhang, Y.; Li, A.; Sun, L. Disposable stainless-steel wire-based electrochemical microsensor for in vivo continuous monitoring of hydrogen peroxide in vein of tomato leaf. *Biosensors* **2022**, *12* (1), 35.

(29) Li, L.; Pan, L.; Ma, Z.; Yan, K.; Cheng, W.; Shi, Y.; Yu, G. All inkjet-printed amperometric multiplexed biosensors based on nanostructured conductive hydrogel electrodes. *Nano Lett.* **2018**, *18* (6), 3322−3327.

(30) Zhai, D.; Liu, B.; Shi, Y.; Pan, L.; Wang, Y.; Li, W.; Yu, G.; Yu, G. Highly sensitive glucose sensor based on Pt nanoparticle/polyaniline hydrogel heterostructures. *ACS Nano* **2013**, *7* (4), 3540−3546.

(31) Yang, M.; Ren, X.; Yang, T.; Xu, C.; Ye, Y.; Sun, Z.; Luo, Z.; Wang, B.; Luo, Z. Polypyrrole/sulfonated multi-walled carbon nanotubes conductive hydrogel for electrochemical sensing of living cells. *Chem. Eng. J.* **2021**, *418*, 129483.

(32) Erfkamp, J.; Guenther, M.; Gerlach, G. Piezoresistive hydrogel-based sensors for the detection of ammonia. *Sensors* **2019**, *19* (4), 971.

(33) Erfkamp, J.; Guenther, M.; Gerlach, G. Enzyme-functionalized piezoresistive hydrogel biosensors for the detection of urea. *Sensors* **2019**, *19* (13), 2858.

(34) Liu, D.; Huyan, C.; Wang, Z.; Guo, Z.; Zhang, X.; Torun, H.; Chen, F.; Xu, B. B.; Chen, F. Conductive polymer-based hydrogels and their application in wearable sensors: A review. *Mater. Horiz.* **2023**, *10* (8), 2800−2823.

(35) Gamboa, J.; Paulo-Mirasol, S.; Estrany, F.; Torras, J. Recent Progress in Biomedical Sensors Based on Conducting Polymer Hydrogels. *ACS Appl. Bio Mater.* **2023**, *6* (5), 1720−1741.

(36) Thakur, V. K.; Thakur, M. K. Recent advances in graft copolymerization and applications of chitosan: A review. *ACS Sustainable Chem. Eng.* **2014**, *2* (12), 2637−2652.

(37) Zhu, J.; Wang, L.; Xu, S.; Peng, L.; Gao, Z.; Liu, S.; Xi, S.; Ma, S.; Cai, W. A high-performance wearable microneedle sensor based on a prussian blue-carbon nanotube composite electrode for the detection of hydrogen peroxide and glucose. *Sens. Actuators, B* **2024**, *419*, 136436.

(38) Zhao, J.; Lv, J.; Ling, G.; Zhang, P. A swellable hydrogel microneedle based on cerium-metal organic frame composite nanozyme for detection of biomarkers. *Int. J. Biol. Macromol.* **2024**, *254*, 127745.

https://doi.org/10.1021/acssensors.4c02645
ACS Sens. XXXX, XXX, XXX−XXX

(39) Yin, Y.; Li, X.; Wang, M.; Ling, G.; Zhang, P. Glucose detection: In-situ colorimetric analysis with double-layer hydrogel microneedle patch based on polyvinyl alcohol and carboxymethyl chitosan. *Int. J. Biol. Macromol.* **2024**, *277*, 134408.
(40) Wu, X.; Pan, Y.; Li, X.; Shao, Y.; Peng, B.; Zhang, C.; Zhang, C.; Yao, S.; Ping, J.; Ying, Y. Rapid and In-Field Sensing of Hydrogen Peroxide in Plant by Hydrogel Microneedle Patch. *Small* **2024**, *20*, 2402024.
(41) Bukhamsin, A.; Lahcen, A. A.; De Oliveira Filho, J.; Shetty, S.; Blilou, I.; Kosel, J.; Salama, K. N. Minimally-invasive, real-time, non-destructive, species-independent phytohormone biosensor for precision farming. *Biosens. Bioelectron.* **2022**, *214*, 114515.
(42) Singh, N.; Kaushik, A.; Ghori, I.; Rai, P.; Dong, L.; Sharma, A.; Malhotra, B. D.; John, R. Electrochemical and plasmonic detection of myocardial infarction using microfluidic biochip incorporated with mesoporous nanoscaffolds. *ACS Appl. Mater. Interfaces* **2024**, *16*, 32794−32811.
(43) Singh, N.; Rai, P.; Ali, M. A.; Kumar, R.; Sharma, A.; Malhotra, B. D.; John, R. A hollow-nanosphere-based microfluidic biosensor for biomonitoring of cardiac troponin I. *J. Mater. Chem. B* **2019**, *7* (24), 3826−3839.
(44) Wang, X.; Jiang, H.; Chen, Y.; Qiao, X.; Dong, L. Microblower-based microfluidic pump. *Sens. Actuators Phys.* **2017**, *253*, 27−34.
(45) Thordal-Christensen, H.; Zhang, Z.; Wei, Y.; Collinge, D. B. Subcellular localization of H_2O_2 in plants. H_2O_2 accumulation in papillae and hypersensitive response during the barley—powdery mildew interaction. *Plant J.* **1997**, *11*, 1187−1194.
(46) Xu, W.; Meng, Y.; Wise, R. P. Mla- and Rom1-mediated control of microRNA398 and chloroplast copper/zinc superoxide dismutase regulates cell death in response to the barley powdery mildew fungus. *New Phytol.* **2014**, *201*, 1396−1412.
(47) Cao, L.; Karapetyan, S.; Yoo, H.; Chen, T.; Mwimba, M.; Zhang, X.; Dong, X. H_2O_2 sulfenylates CHE, linking local infection to the establishment of systemic acquired resistance. *Science* **2024**, *385* (6714), 1211−1217.
(48) Szabó, T.; Berkesi, O.; Forgó, P.; Josepovits, K.; Sanakis, Y.; Petridis, D.; Dékány, I. Evolution of surface functional groups in a series of progressively oxidized graphite oxides. *Chem. Mater.* **2006**, *18* (11), 2740−2749.
(49) Masud, R. A.; Islam, M. S.; Haque, P.; Khan, M. N. I.; Shahruzzaman, M.; Khan, M.; Rahman, M. M.; Rahman, M. M. Preparation of novel chitosan/poly (ethylene glycol)/ZnO bionanocomposite for wound healing application: Effect of gentamicin loading. *Materialia* **2020**, *12*, 100785.
(50) Nanda, R.; Sasmal, A.; Nayak, P. L. Preparation and characterization of chitosan−polylactide composites blended with Cloisite 30B for control release of the anticancer drug paclitaxel. *Carbohydr. Polym.* **2011**, *83* (2), 988−994.
(51) Namli, H.; Turhan, O. Background defining during the imine formation reaction in FT-IR liquid cell. Spectrochimica Acta Part A: *Mol. Biomol. Spectrosc.* **2006**, *64* (1), 93−100.
(52) Nainggolan, I.; Agusnar, H.; Alfian, Z.; Alva, S.; Nasution, T. I.; Rahman, R.; Sembiring, A. Sensitivity of Chitosan Film Based Electrode Modified with Reduced Graphene Oxide (rGO) for Formaldehyte Detection Using Cyclic Voltammetry. *S. Afr. J. Chem. Eng.* **2024**, *48* (1), 184−193.
(53) Shin, J.-H.; Lee, M.-J.; Choi, J.-H.; Song, J.-A.; Kim, T.-H.; Oh, B.-K. Electrochemical H_2O_2 biosensor based on horseradish peroxidase encapsulated protein nanoparticles with reduced graphene oxide-modified gold electrode. *Nano Converg.* **2020**, *7* (1), 39.
(54) Singh, N.; Khan, R. R.; Xu, W.; Whitham, S. A.; Dong, L. Plant Virus Sensor for the Rapid Detection of Bean Pod Mottle Virus Using Virus-Specific Nanocavities. *ACS Sens.* **2023**, *8* (10), 3902−3913.
(55) Yao, H.; Li, N.; Wei, Y. L.; Zhu, J. J. A H2O2 biosensor based on immobilization of horseradish peroxidase in a gelatine network matrix. *Sensors* **2005**, *5* (4), 277−283.
(56) Maehly, A. C. *Plant peroxidases: methods in Enzymology*; Academic Press: New York, 1995; Vol. *11*, pp. 807.
(57) Wu, S. H.; Huang, X. B.; Tang, Y.; Ma, L. M.; Liu, Y.; Sun, J. J. Temperature controllable electrochemical sensors based on horseradish peroxidase as electrocatalyst at heated Au disk electrode and its preliminary application for H2O2 detection. *Anal. Chim. Acta.* **2020**, *1096*, 44−52.
(58) https://assets.thermofisher.com/TFS-Assets/LPD/Product-Information/Why-How-Matrix-Spike-ST-MATSPIKE-EN.pdf.
(59) Daudi, A.; O'brien, J. A. Detection of hydrogen peroxide by DAB staining in Arabidopsis leaves. *Bio-Protocol.* **2012**, *2* (18), 263−263.
(60) Donaldson, L. Autofluorescence in plants. *Molecules* **2020**, *25* (10), 2393.
(61) https://bjbmaterials.com/wc-783-a-b/.
(62) Tian, Y.; Zeng, Z.; Gong, H.; Zhou, Y.; Qi, L.; Zhen, W. Simulation of tensile behavior of tobacco leaf using the discrete element method (DEM. *Computers Electron. Agric.* **2023**, *205*, 107570.
(63) Kaçar, C.; Dalkiran, B.; Erden, P. E.; Kiliç, E. An amperometric hydrogen peroxide biosensor based on Co_3O_4 nanoparticles and multiwalled carbon nanotube modified glassy carbon electrode. *Appl. Surf. Sci* **2014**, *311*, 139−146.
(64) Chen, X.; Chen, Z.; Zhu, J.; Xu, C.; Yan, W.; Yao, C. A novel H_2O_2 amperometric biosensor based on gold nanoparticles/self-doped polyaniline nanofibers. *Bioelectrochemistry* **2011**, *82* (2), 87−94.
(65) Liu, H.; Guo, K.; Duan, C.; Chen, X.; Zhu, Z. A novel biosensor based on the direct electrochemistry of horseradish peroxidase immobilized in the three-dimensional flower-like Bi2WO6 microspheres. *Mater. Sci. Eng., C* **2016**, *64*, 243−248.
(66) Thenmozhi, K.; Narayanan, S. S. Horseradish peroxidase and toluidine blue covalently immobilized leak-free sol-gel composite biosensor for hydrogen peroxide. *Mater. Sci. Eng., C* **2017**, *70*, 223−230.
(67) Zhan, B.; Liu, C.; Shi, H.; Li, C.; Wang, L.; Huang, W.; Dong, X. A hydrogen peroxide electrochemical sensor based on silver nanoparticles decorated three-dimensional graphene. *Appl. Phys. Lett.* **2014**, *104* (24), 24.
(68) Ren, Q. Q.; Yuan, X. J.; Huang, X. R.; Wen, W.; Zhao, Y. D.; Chen, W. In vivo monitoring of oxidative burst on aloe under salinity stress using hemoglobin and single-walled carbon nanotubes modified carbon fiber ultramicroelectrode. *Biosens. Bioelectron.* **2013**, *50*, 318−324.
(69) Yin, S.; Dong, L. Plant tattoo sensor array for leaf relative water content, surface temperature, and bioelectric potential monitoring. *Adv. Mater. Technol.* **2024**, *9* (12), 2302073.
(70) Ibrahim, H.; Moru, S.; Schnable, P.; Dong, L. Wearable plant sensor for in situ monitoring of volatile organic compound emissions from crops. *ACS Sens.* **2022**, *7* (8), 2293−2302.
(71) Ibrahim, H.; Yin, S.; Moru, S.; Zhu, Y.; Castellano, M. J.; Dong, L. In planta nitrate sensor using a photosensitive epoxy bioresin. *ACS Appl. Mater. Interfaces* **2022**, *14* (22), 25949−25961.
(72) Yin, S.; Ibrahim, H.; Schnable, P. S.; Castellano, M. J.; Dong, L. A field-deployable, wearable leaf sensor for continuous monitoring of vapor-pressure deficit. *Adv. Mater. Technol.* **2021**, *6* (6), 2001246.
(73) Rahman, M. T.; Khan, R. R.; Tian, Y.; Ibrahim, H.; Dong, L. High-sensitivity and room-temperature nitrous oxide sensor using Au nanoparticles-decorated MoS_2. *IEEE Sens. J.* **2023**, *23* (17), 18994−19001.
(74) Yin, H.; Cao, Y.; Marelli, B.; Zeng, X.; Mason, A. J.; Cao, C. Soil sensors and plant wearables for smart and precision agriculture. *Adv. Mater.* **2021**, *33* (20), 2007764.
(75) Du, H.; Li, X.; Yao, P.; Wang, J.; Sun, Y.; Dong, L. Zinc oxide coated tin oxide nanofibers for improved selective acetone sensing. *Nanomaterials* **2018**, *8* (7), 509.
(76) Chen, Y.; Tian, Y.; Wang, X.; Wei, L.; Dong, L. Miniaturized, field-deployable, continuous soil water potential sensor. *IEEE Sens. J.* **2020**, *20* (23), 14109−14117.
(77) Zhu, Y.; Chen, Y.; Ali, M. A.; Dong, L.; Wang, X.; Archontoulis, S. V.; Schnable, J. C.; Castellano, M. J. Continuous in situ soil nitrate sensors: The importance of high-resolution measurements across time

https://doi.org/10.1021/acssensors.4c02645
ACS Sens. XXXX, XXX, XXX−XXX

and a comparison with salt extraction-based methods. *Soil Sci. Soc. Am. J.* **2021**, *85* (3), 677−690.
(78) Kumar, S. A.; Ilango, P. The impact of wireless sensor network in the field of precision agriculture: A review. *Wireless Personal Commun.* **2018**, *98*, 685−698.

https://doi.org/10.1021/acssensors.4c02645
ACS Sens. XXXX, XXX, XXX−XXX